Deep Learning-Based Galls and Healthy Leaf Recognition Using Depthwise Separable CNN Architecture

Imam Yuadi
Department of Information and Library Science, Airlangga University, Surabaya, Indonesia
imam.yuadi@fisip.unair.ac.id (corresponding author)

Nisak Ummi Nazikhah
Department of Natural Science Education, Hasyim Asy'ari University, Indonesia
nisakumminazikhah@mhs.unhasy.ac.id

Chih-Chien Hu
Department of Information Management, Tatung University, Taipei, Taiwan
holdenhu@gm.ttu.edu.tw

Khoirun Nisa'
Department of Information and Library Science, Airlangga University, Surabaya, Indonesia
khoirun.nisa-2017@fisip.unair.ac.id

Vasanthadev S. Suryakala
Department of Electronics & Communication, Faculty of Engineering & Technology, SRM Institute of Science and Technology, Kattankulathur, Chennai, India
suryakas@srmist.edu.in

Received: 26 March 2025 | Accepted: 1 May 2025

 DOI: https://doi.org/10.48084/etasr.11142

ABSTRACT

Alstonia scholaris plays an important role in tropical ecosystems, contributing to soil conservation and carbon sequestration. However, it is susceptible to pest infestations, especially galls caused by a variety of factors, which can affect the growth and health of plants. This study employed a deep learning approach to classify healthy and gall-affected leaves using CNN with Depthwise Separable Convolution (DSC). A dataset consisting of 11,800 leaf images was processed with various augmentation and filtering techniques to evaluate their effect on classification performance. The experimental results indicated that the optimized filter achieved the highest accuracy (99.3%) in differentiating between healthy leaves and leaves affected by galls. The CNN model utilizing DSC was selected for its ability to significantly decrease computational complexity while maintaining classification accuracy, making it suitable for efficient image analysis jobs. This study shows that deep learning could function as an effective option for the early detection of plant diseases. Future investigations should examine transfer learning and multispectral imaging methods to improve model adaptability and classification precision.

Keywords-alstonia scholaris; plants; CNN depthwise separable convolution; image preprocessing

I. INTRODUCTION

The leaves of Alstonia scholaris, commonly referred to as the pulai tree, are essential for tropical ecosystems [1]. Alstonia scholaris, a tree characterized by its erect greenish stems and white blossoms, is recognized by its elliptical leaves [2]. Bark comprises active chemicals, including alkaloids and flavonoids, which exhibit antiparasitic, anti-inflammatory, and immunostimulatory activities. In addition, its wood fibers are highly suitable for producing high-quality paper, offering excellent ink absorption and texture [3]. Pulai trees also facilitate the absorption of carbon dioxide from the atmosphere, making them significant contributors in the fight against climate change. Its leaves demonstrate significant antioxidant activity, aiding in the protection of cells from oxidative stress and premature aging [4]. However, the tree is vulnerable to environmental changes, as climate change and declining circumstances have increased the risk of pests and diseases, particularly leaf galls. Although typically not lethal, severe gall infestations can impede tree development and photosynthesis, compromising its overall vitality [5]. This presents a major concern in agriculture and forestry, where gall-induced damage can lead to economic losses. Leaf galls have been extensively studied to understand their causes, consequences, and management strategies. For instance, in [6], Paurosylla tuberculata was found to be the primary insect generating galls on Alstonia scholaris leaves. Gall assaults can hinder the development of six-month-old seedlings and inflict obvious damage on the plants [7]. In recent years, deep learning and computer vision have shown great promise in the identification of plant diseases. For galls on Cordia leaves, several models were tested in [8], including modified Yolov4, Yolov5, Yolov7, and SSD, achieving good levels of accuracy. In [9], Recurrent Neural Networks (RNN) were used to detect galls on various plants. Using these technologies to build models that can distinguish between healthy and sick leaves can improve pest control using early identification, including those endangering the health of the pulai tree.

Improving the accuracy of digital image analysis-based plant disease diagnosis is based mainly on image preprocessing to improve segmentation, feature extraction, and background elimination. Such methods minimize noise that can interfere with categorization while emphasizing significant portions of leaf pictures [10]. For instance, in [11], image preprocessing methods, including scaling and pixel normalization on a Kaggle dataset with 536 classes, helped achieve a high validation accuracy of 95% in recognizing potato leaf disorders. Research on maize plant disease detection has emphasized the need for techniques such as neighborhood average, median filtering, and spatial low-pass filtering to help isolate impacted areas on leaves and increase the accuracy of Support Vector Machine (SVM) models [12].

This study sought to explore key questions: How effective is a Convolutional Neural Network (CNN) with Depthwise Separable Convolution (DSC) in identifying gall-infected leaves? What image preprocessing techniques are most effective in improving the accuracy of gall detection? The novelty of this research is its specific focus on using a deep learning-based CNN with DSC, a method that has received little attention in previous research. Through this approach, the study aims to contribute meaningfully to the development of automated plant disease detection systems, particularly to support the conservation and productivity of pulai plants.

II. METHODS

This study presents a structured approach to analyze and classify Alstonia scholaris leaf images using image processing. Figure 1 shows a flowchart of this study, which used 11,800 high-resolution images labeled as galled or healthy.

A. Dataset Acquisition

Leaf images were captured using a Vivo smartphone at 3072×4096 resolution. These images were then preprocessed through cropping and segmentation, as shown in Figure 2, to isolate the Region of Interest (ROI) and enhance image quality for analysis.

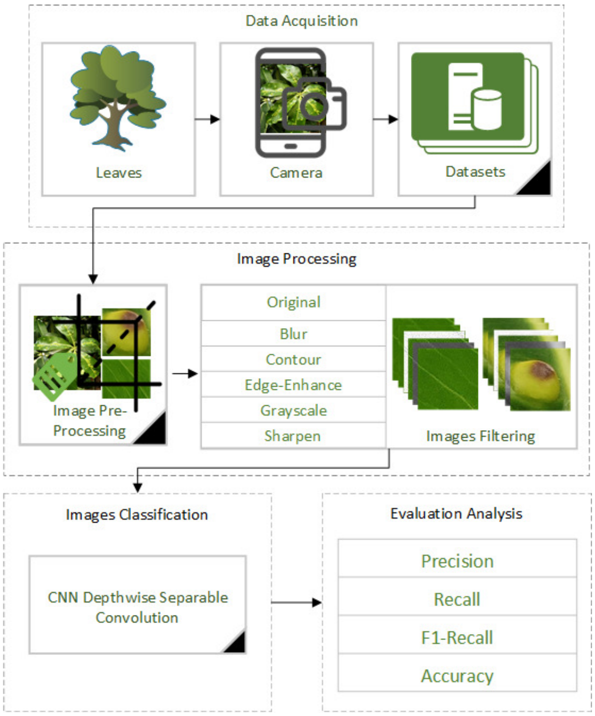

Fig. 1. Flowchart of the proposed method.

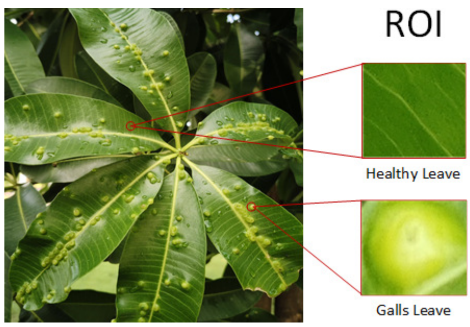

Fig. 2. Region of Interest (RoI) of healthy and gall leaves.

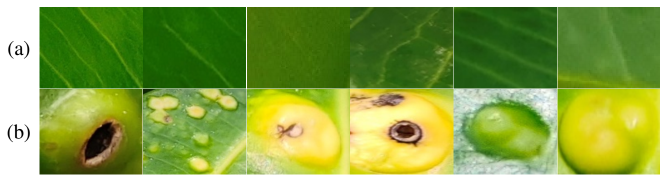

Fig. 3. Dataset sample: (a) health leaves, (b) galls leaves.

A total of 2,226 images were collected, evenly divided between healthy and gall-affected leaves. This balanced dataset supports reliable model training and evaluation. Figure 3 shows sample images of both categories. To enhance training data and prevent overfitting, various image augmentation techniques were applied using Keras' Image Data Generator. These included rotation, shifting, shearing, zooming, and flipping, which helped the model learn from diverse leaf variations and adapt to real-world conditions. As a result, the dataset was expanded to 11,800 images, evenly divided between healthy and gall-affected leaves.

B. Image Processing

After collection, the images were stored and enhanced using filters such as Blur, Contour, Edge enhancement, Grayscale, and Sharpening. These filters help highlight important features, making the images clearer and easier for the system to process in the next stage.

- The Blur filter is used to smooth an image by smoothing out changes in the intensity of surrounding pixels [13]. One such method, used in this experiment, is Gaussian, which uses the Gaussian function to smooth out sharp changes in an image. The formula used in Gaussian blur is:

$$G(x, y) = \frac{1}{2\pi\sigma^2} e^{-\frac{x^2+y^2}{2\sigma^2}} \quad (1)$$

where $G(x, y)$ is the Gaussian function implemented on pixel (x, y), and σ is the standard deviation obtained from the Gaussian distribution, controlling the blur level.

- Contour filter: To bring out the edges or outlines in an image, a contour filter helps by picking up on noticeable changes in brightness between neighboring pixels [14, 15]. One commonly used method for this is the Sobel filter, which works by applying a special kind of mathematical operation, called convolution, to measure how the brightness shifts both side-to-side and up-and-down. The Sobel Kernel was used to detect these contours:

$$C_x = \begin{bmatrix} -1 & 0 & 1 \\ -2 & 0 & 2 \\ -1 & 0 & 1 \end{bmatrix}, \quad C_y = \begin{bmatrix} -1 & -2 & -1 \\ 0 & 0 & 0 \\ 1 & 2 & 1 \end{bmatrix} \quad (2)$$

The gradient magnitude is calculated as follows:

$$C = \sqrt{C_x^2 + C_y^2} \quad (3)$$

where C_x and C_y represent the slopes in the horizontal and vertical directions, respectively. C is the gradient magnitude value that indicates the strength of intensity variations at the image's edges.

- Edge enhancement increases the contrast in places with strong intensity variations [16], thus improving edges in an image. The Laplacian filter is one of the techniques applied in this experiment, which detects intensity variations using the Laplacian operator:

$$\nabla^2 f(x, y) = \frac{\{\partial^2 f\}}{\{\partial x^2\}} + \frac{\{\partial^2 f\}}{\{\partial y^2\}} \quad (4)$$

where $\nabla^2 f(x, y)$ is the second differential operator applied in the edge-enhanced filter to emphasize picture pixel intensity changes, and $\frac{\{\partial^2 f\}}{\{\partial x^2\}}$ and $\frac{\{\partial^2 f\}}{\{\partial y^2\}}$ are the second partial derivative about the horizontal (x) and vertical (y) axes, respectively. Detecting and emphasizing the edges of an object depends much on this calculation, which seeks to measure the change in intensity in an image area.

- A grayscale filter converts images into black-and-white images. This filter removes color information and retains only the pixel intensities [17]. The RGB to grayscale conversion formula was:

$$I = 0.2989R + 0.5870G + 0.1140B \quad (5)$$

where I is the grayscale intensity value, and R, G, and B are the intensity values of the red, green, and blue components in the image, respectively.

- A Sharpen filter is used to increase the sharpness of an image by clarifying details and increasing the contrast between adjacent pixels [18]. One such method used was unsharp masking, using the following formula for 3×3 kernel sharpening:

$$\begin{bmatrix} 0 & -1 & 0 \\ -1 & 5 & -1 \\ 0 & -1 & 0 \end{bmatrix} \quad (6)$$

This kernel enhances the center pixel and reduces the influence of surrounding pixels to produce a sharper image. The center pixel value is amplified with a large positive weight, which is 5, while the surrounding pixels are given a negative weight (-1) to produce a sharpening effect. Thus, the features in the image become clearer and easier to recognize. In image processing, this filter is extensively applied to improve the visibility of significant features before additional studies, such as image segmentation or pattern recognition.

C. Image Classification

A CNN with DSC was used to classify the data. This approach was selected for its ability to automatically extract important elements from images, thus eliminating the requirement for human feature extraction methods [19]. The CNN structure, shown in Figure 4, uses DSC to handle image data. This begins with an input image of 150×150 with three color channels passing through a sequence of SeparableConv2D layers with rising filter sizes (32, 64, and 128), each followed by a max pooling layer to downplay the spatial dimensions using 10 epochs. During training, a batch size of 32 was employed to balance model convergence speed and memory efficiency, which is appropriate given the input size and model complexity.

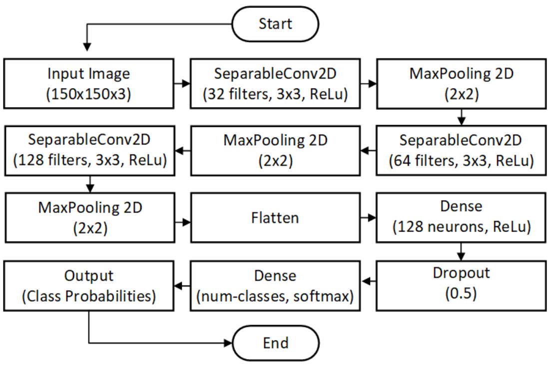

Fig. 4. Flowchart of the proposed method.

Following feature extraction, the data was flattened into a 1D vector and subjected to ReLU activation through a 128-neuron dense layer. To avoid overfitting, a Dropout layer with a rate of 0.5 was added before the final output layer, which used softmax activation to produce class probabilities.

D. Evaluation Analysis

In this stage, confusion matrix results and related metrics were used to measure the accuracy of each algorithm. This helps visualize how many data points are correctly or incorrectly classified. By using the test and score widget, the performance of the three algorithms was evaluated through key metrics, such as accuracy, precision, recall, and F1 score. Classification Accuracy (CA), one of the most common metrics in machine learning, shows the percentage of data correctly predicted by the model [20]:

$$CA = \frac{TP+FN}{TP+TN+FN+FP} \tag{7}$$

In this context, TP and TN refer to correctly predicted outcomes for positive and negative classes, respectively. FP are cases wrongly predicted as positive, while FN are actual positives incorrectly predicted as negative. These values help determine the model's performance.

Precision measures how accurate the model is when predicting positive results [20]:

$$Precision = \frac{TP}{TP+FP} \tag{8}$$

Recall shows how well the model can detect all actual positive cases [20], calculated by:

$$Recall = \frac{TP}{TP+FN} \tag{9}$$

The F1 score combines precision and recall into one metric, offering a balanced measure of a model's classification performance. This metric is especially useful when dealing with uneven class distributions [21], and is calculated as follows:

$$F1 = 2 \times \frac{Precision \times Recall}{Precision + Recall} \tag{10}$$

III. RESULTS AND DISCUSSION

This study used image processing to highlight differences between healthy and diseased leaves. Filters enhanced key features, helping to identify them more easily, as shown in Figure 5.

The original image achieved high accuracy (0.989 and 0.987) with balanced precision and recall. The Blur filter maintained strong performance, with an F1 score of 0.992 and a slight increase in accuracy. The Contour filter decreased the recall of class "a" (0.942) and its F1 score (0.961), while class "b" remained high (0.992). The Edge enhancement filter slightly decreased the recall but increased the precision, keeping the F1 score at 0.991. The Grayscale filter decreased accuracy the most (0.968 and 0.969), possibly due to loss of color information. In contrast, the Sharpen filter increased precision and accuracy the most (0.993 and 0.994), indicating the best classification performance. These findings are in line with [22], which highlighted the importance of feature preservation in plant disease detection based on two-way residual dense layers. In this module, a separable depth convolution was introduced, which reduced the amount of parameter calculation and achieved a performance of over 98%.

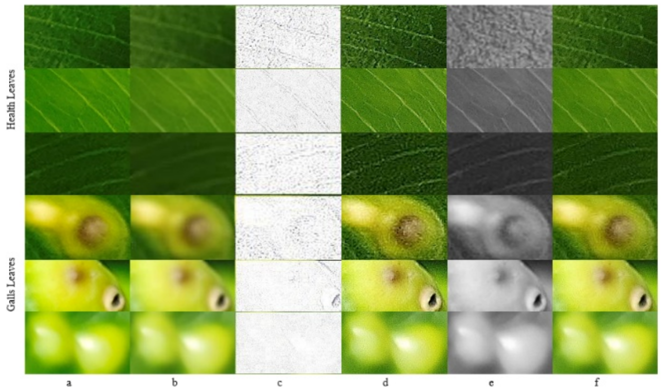

Fig. 5. Image filtering results: (a) original, (b) blur, (c) contour, (d) edge enhancement, (e) grayscale, (f) sharpen.

Table I shows the results of using different image filters. These metrics help show how effectively each filter preserves important image features and supports accurate classification.

TABLE I. RESULT OF IMAGE CLASSIFICATION EACH FILTER IN (A) GALLS CLASS(B) HEALTH CLASS

Filters	Class	Precision	Recall	F1-score	Accuracy
Original	a	0.981	0.993	0.992	0.989
	b	0.992	0.981	0.992	0.987
Blur	a	0.993	0.992	0.992	0.992
	b	0.992	0.993	0.992	0.993
Contour	a	0.992	0.942	0.961	0.997
	b	0.943	0.992	0.962	0.964
Edge enhancement	a	0.999	0.983	0.991	0.989
	b	0.982	0.999	0.991	0.989
Grayscale	a	0.972	0.971	0.973	0.968
	b	0.973	0.972	0.971	0.969
Sharpen	a	0.998	0.992	0.993	0.993
	b	0.993	0.998	0.992	0.994

Figure 6 shows that the original and sharpened filters achieved the most stable and high validation accuracy, suggesting well-balanced models. Blur and Edge enhancement performed well, although the latter showed slight overfitting. Meanwhile, grayscale and contour filters led to unstable results due to possible loss of key visual features. Overall, the Sharpen and Original filters were the most reliable for classification. Compared to traditional methods such as SVM, CNN performed better in [23], achieving 95.33% accuracy compared to 85.07% for SVM. This was further supported in [24], where lightweight CNN models maintained high accuracy while offering better efficiency in processing speed [25].

Figure 7 illustrates the influence of various image filters on classification accuracy using confusion matrices. Sharpen exhibited optimal performance, yielding merely 11 FP and 2 FN, hence augmenting critical details for improved recognition.

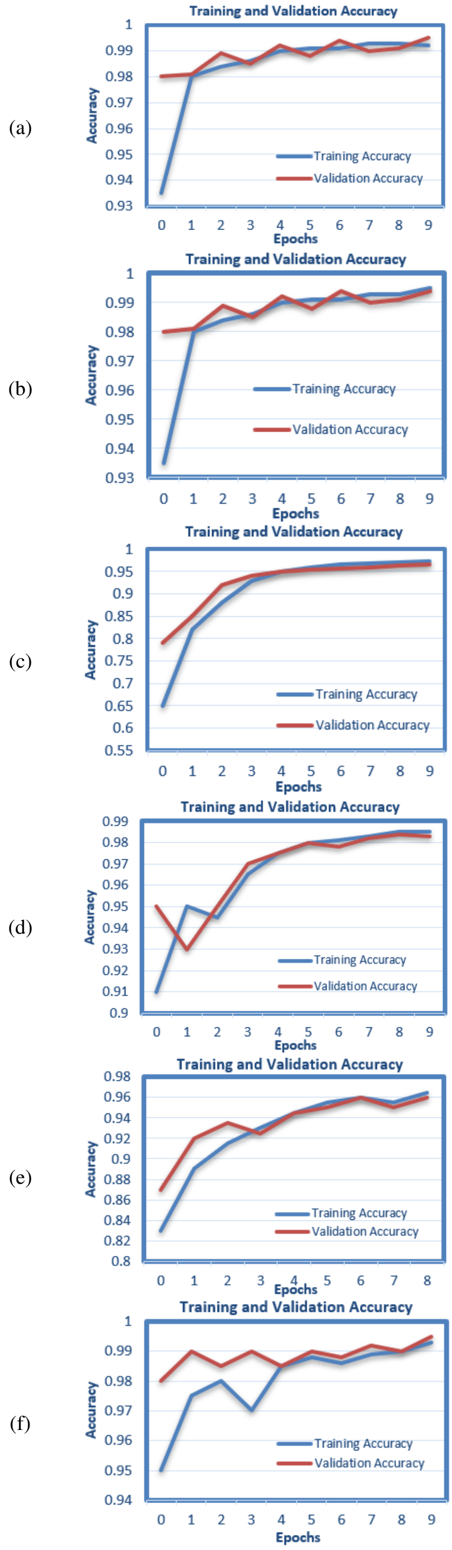

Fig. 6. Training and validation accuracy (a) Original (b) Blur (c) Contour (d) Edge enhancement, (e) Grayscale, (f) Sharpen.

Blur and Edge Enhancement are nearly aligned, balancing noise reduction and feature clarity while adding marginally more inaccuracies. Grayscale resulted in a little reduction in accuracy by eliminating color information, thus complicating disease differentiation. Contour exhibited the poorest performance, exacerbating misclassifications by accentuating edges at the expense of critical textures. In summary, Sharpen demonstrated superior efficacy but Contour impeded precision. Selecting the appropriate filter is essential for enhancing model performance. In line with [26], which used Excess Green Index (ExG) and Few-Shot Learning for more robust and scalable disease detection, this study presents an innovative way CNN with DSC that offers benefits in the detection of healthy and diseased Alstonia scholaris leaves. Furthermore, the image processing techniques in this study were proven to increase accuracy. This is similar to [27, 28], which used image processing techniques in the form of multiscale feature extraction methods to increase the accuracy of plant disease detection models.

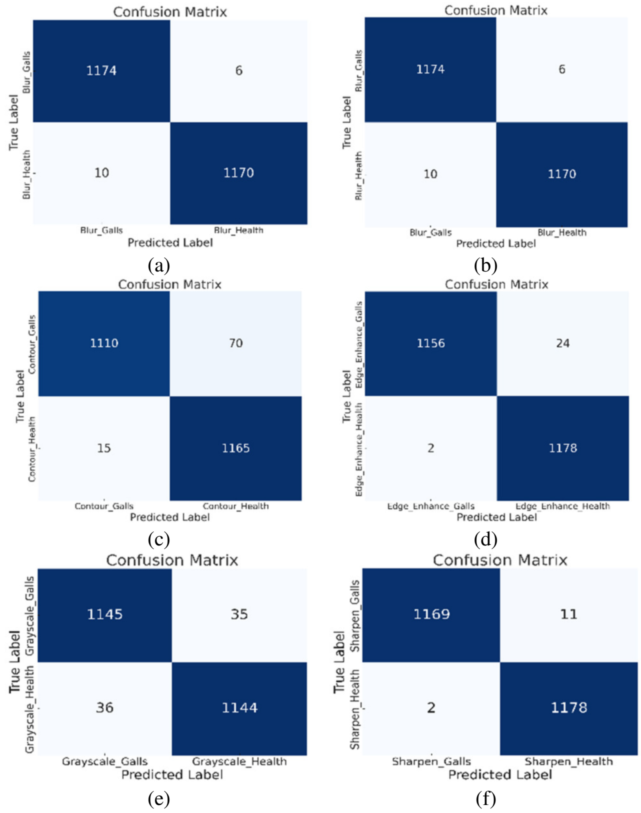

Fig. 7. Confusion matrices: (a) Original, (b) Blur, (c) Contour, (d) Edge Enhance, (e) Grayscale, (f) Sharpen.

IV. CONCLUSION

This study demonstrated that CNN with DSC effectively classified healthy and gall-affected leaves of Alstonia scholaris. The Sharpen filter produced the highest classification accuracy by improving critical visual features. These results highlight the importance of meticulous image preprocessing to improve deep learning model performance. CNN-DSC offers a promising approach to early detection and management of plant diseases in Alstonia scholaris. Future studies should explore multispectral imaging to capture more subtle disease symptoms. The application of transfer learning and advanced data augmentation techniques could further enhance model robustness.

ACKNOWLEDGMENT

This work is supported by the SATU Joint Research Scheme (JRS) Airlangga Research Fund 2022 Program with the title VISION INTELLIGENCE IN LIFE SCIENCES based on the Decree of the Chancellor of Airlangga University with Grant Number 607/UN3.15/PT/2022.

REFERENCES

[1] H. Singh, "An integrated approach considering physiological- and biophysical-based indicators for assessing tolerance of roadside plantations of Alstonia scholaris towards urban roadside air pollution: an assessment of adaptation of plantations for mitigating roadside air pollution," *Trees*, vol. 37, no. 1, pp. 69–83, Feb. 2023, https://doi.org/10.1007/s00468-021-02179-8.

[2] S. Sookying, A. Panase, P. Srisuttha, A. Chaophothun, and P. Panase, "Devil's tree flower (*Alstonia scholaris*) extract: positive effects on growth performance and serum biochemical indices in *Channa striata* (Bloch, 1793)," *Journal of Applied Animal Research*, vol. 51, no. 1, pp. 677–683, Dec. 2023, https://doi.org/10.1080/09712119.2023.2273279.

[3] A. Majid and H. R. Faraj, "A review Study of The Chemical Constituents and Pharmacological Activities of Alstonia scholaris linn," *University of Thi-Qar Journal of Science*, vol. 10, no. 1, pp. 81–86, Jun. 2023, https://doi.org/10.32792/utq/utjsci/v10i1.934.

[4] Ka. Chowdary and R. Jash, "Ethanolic extracts of Alstonia Scholaris and Bacopa Monniera possess neuroleptic activity due to anti-dopaminergic effect," *Pharmacognosy Research*, vol. 6, no. 1, 2014, Art. no. 46, https://doi.org/10.4103/0974-8490.122917.

[5] K. Pandey and A. S. Kate, "Comparative analysis of foliar galls and ungalled leaves of Alstonia scholaris with a focus on tissue ultrastructure and phytochemistry," *Biochemical Systematics and Ecology*, vol. 115, Aug. 2024, Art. no. 104851, https://doi.org/10.1016/j.bse.2024.104851.

[6] O. P. Datta and S. C. Datta, "Studies on the histomorphology of leaf galls on Alstonia scholaris L. (Apocynaceae) induced by Pauropsylla tuberculata Crawford," *International Journal of Agricultural Invention*, vol. 1, no. 01, pp. 65–70, Jun. 2016, https://doi.org/10.46492/IJAI/2016.1.1.10.

[7] A. Muhammad, N. Kumar, I. I. Dangora, I. I. Muhammad, A. Mathur, and M. Abdulhamid, "Incidence, severity and biochemical studies of Alstonia scholaris (L.) R. Br. Foliar Galls," *International Journal of Plant Pathology and Microbiology*, vol. 3, no. 2, pp. 7–12, 2023.

[8] M. Ayaz *et al.*, "Automatic Early Diagnosis of Dome Galls in Cordia Dichotoma G. Forst. Using Deep Transfer Learning," *IEEE Access*, vol. 11, pp. 59511–59523, 2023, https://doi.org/10.1109/ACCESS.2023.3283568.

[9] R. Harsha, S. Karthika, M. Priya D, R. Kanna P, G. Rajeshkumar, and E. Mythili, "Folla Disease Detection using In-Depth Learning," in *2023 2nd International Conference on Applied Artificial Intelligence and Computing (ICAAIC)*, Salem, India, May 2023, pp. 547–552, https://doi.org/10.1109/ICAAIC56838.2023.10141305.

[10] M. Dias and C. T. Lopes, "Optimization of Image Processing Algorithms for Character Recognition in Cultural Typewritten Documents," *Journal on Computing and Cultural Heritage*, vol. 16, no. 4, pp. 1–25, Dec. 2023, https://doi.org/10.1145/3606705.

[11] M. B. E. Luogon and F. Al-Turjman, "Cassava leave disease image classification based on deep convolutional neural network," in *Artificial Intelligence of Things (AIoT)*, Elsevier, 2025, pp. 65–72.

[12] T. Ren, Y. Zhang, and C. Wang, "Identification of Corn Leaf Disease Based on Image Processing," in *2019 2nd International Conference on Information Systems and Computer Aided Education (ICISCAE)*, Dalian, China, Sep. 2019, pp. 165–168, https://doi.org/10.1109/ICISCAE48440.2019.221610.

[13] Y. Q. Liu, X. Du, H. L. Shen, and S. J. Chen, "Estimating Generalized Gaussian Blur Kernels for Out-of-Focus Image Deblurring," *IEEE Transactions on Circuits and Systems for Video Technology*, vol. 31, no. 3, pp. 829–843, Mar. 2021, https://doi.org/10.1109/TCSVT.2020.2990623.

[14] P. A. Lyakhov, A. S. Abdulsalyamova, M. R. Kiladze, D. I. Kaplun, and A. S. Voznesensky, "Method of Oriented Contour Detection on Image Using Lorentz Function," in *2020 9th Mediterranean Conference on Embedded Computing (MECO)*, Budva, Montenegro, Jun. 2020, pp. 1–4, https://doi.org/10.1109/MECO49872.2020.9134224.

[15] R. Ratajczak, C. F. Crispim-Junior, E. Faure, B. Fervers, and L. Tougne, "Automatic Land Cover Reconstruction From Historical Aerial Images: An Evaluation of Features Extraction and Classification Algorithms," *IEEE Transactions on Image Processing*, vol. 28, no. 7, pp. 3357–3371, Jul. 2019, https://doi.org/10.1109/TIP.2019.2896492.

[16] W. Li, Z. Zhao, J. Du, and Y. Wang, "Edge-Preserve Filter Image Enhancement with Application to Medical Image Fusion," *Journal of Medical Imaging and Health Informatics*, vol. 7, no. 1, pp. 16–24, Feb. 2017, https://doi.org/10.1166/jmihi.2017.1980.

[17] L. Zhang and Y. Wan, "Color-to-gray image conversion using salient colors and radial basis functions," *Journal of Electronic Imaging*, vol. 33, no. 01, Feb. 2024, https://doi.org/10.1117/1.JEI.33.1.013047.

[18] B. J. Borah and C. K. Sun, "A GPU-Accelerated Modified Unsharp-Masking Method for High-Frequency Background- Noise Suppression," *IEEE Access*, vol. 9, pp. 68746–68757, 2021, https://doi.org/10.1109/ACCESS.2021.3077287.

[19] R. Zhang, F. Zhu, J. Liu, and G. Liu, "Depth-Wise Separable Convolutions and Multi-Level Pooling for an Efficient Spatial CNN-Based Steganalysis," *IEEE Transactions on Information Forensics and Security*, vol. 15, pp. 1138–1150, 2020, https://doi.org/10.1109/TIFS.2019.2936913.

[20] S. Sathyanarayanan, "Confusion Matrix-Based Performance Evaluation Metrics," *African Journal of Biomedical Research*, pp. 4023–4031, Nov. 2024, https://doi.org/10.53555/AJBR.v27i4S.4345.

[21] S. Farhadpour, T. A. Warner, and A. E. Maxwell, "Selecting and Interpreting Multiclass Loss and Accuracy Assessment Metrics for Classifications with Class Imbalance: Guidance and Best Practices," *Remote Sensing*, vol. 16, no. 3, Jan. 2024, Art. no. 533, https://doi.org/10.3390/rs16030533.

[22] L. Liao, B. Li, and J. Tang, "Plants Disease Image Classification Based on Lightweight Convolution Neural Networks," *International Journal of Pattern Recognition and Artificial Intelligence*, vol. 36, no. 13, Oct. 2022, Art. no. 2254013, https://doi.org/10.1142/S0218001422540131.

[23] A. Patil, "Plant Leaf Disease Classification Using SVM and CNN Algorithms," *International Journal of Food And Nutrutional Sciences*, vol. 11, no. 13, pp. 223–227, Nov. 2022.

[24] K. Kc, Z. Yin, M. Wu, and Z. Wu, "Depthwise separable convolution architectures for plant disease classification," *Computers and Electronics in Agriculture*, vol. 165, Oct. 2019, Art. no. 104948, https://doi.org/10.1016/j.compag.2019.104948.

[25] R. H. Altaie and H. K. Hoomod, "An Intrusion Detection System using a Hybrid Lightweight Deep Learning Algorithm," *Engineering, Technology & Applied Science Research*, vol. 14, no. 5, pp. 16740–16743, Oct. 2024, https://doi.org/10.48084/etasr.7657.

[26] S. Saleem, M. I. Sharif, M. I. Sharif, M. Z. Sajid, and F. Marinello, "Comparison of Deep Learning Models for Multi-Crop Leaf Disease Detection with Enhanced Vegetative Feature Isolation and Definition of a New Hybrid Architecture," *Agronomy*, vol. 14, no. 10, Sep. 2024, Art. no. 2230, https://doi.org/10.3390/agronomy14102230.

[27] M. A. Naeem *et al.*, "Deep Learning-Based Approach for Identification of Potato Leaf Diseases Using Wrapper Feature Selection and Feature Concatenation." arXiv, Apr. 29, 2025, https://doi.org/10.48550/arXiv.2502.03370.

[28] S. Saleem, A. Hussain, N. Majeed, Z. Akhtar, and K. Siddique, "A Multi-Scale Feature Extraction and Fusion Deep Learning Method for Classification of Wheat Diseases," *Journal of Computer Science*, vol. 21, no. 1, pp. 34–42, Jan. 2025, https://doi.org/10.3844/jcssp.2025.34.42.